Examining the utility of epoxy replicas of single, natural fractures in dolostone for visualization experiments

Journal:	*Hydrogeology Journal*
Manuscript ID:	HJ-2006-0279.R2
Category:	Paper
Date Submitted by the Author:	n/a
Complete List of Authors:	Bergslien, Elisa; Buffalo State College, Earth Sciences and Science Education Fountain, John; North Carolina State University, Department of Marine, Earth and Atmopsheric Sciences
Keywords:	fractured rocks, groundwater flow, scale effects, physical modeling, aperture statistics

Examining the utility of epoxy replicas of single, natural fractures in dolostone for visualization experiments

Elisa Bergslien
Earth Science and Science Education Department, 217 Science Building, Buffalo State College, Buffalo, New York. 14222 bergslet@buffalostate.edu (716) 878-793 fax: (716) 878-4524

John Fountain
Department of Marine, Earth and Atmospheric Sciences, 2800 Faucette Drive, Rm. 1125 Jordan Hall, North Carolina State University, Raleigh, North Carolina, 27695-8208

Abstract

Epoxy casts were created of five naturally occurring fractures in dolostone and aperture distribution was measured using a light attenuation method. The optically determined aperture matrices showed a skew towards smaller apertures, with the larger models demonstrating a lognormal distribution and the smaller models a normal distribution. Surface variograms of each display a significant degree of anisotropy. The models had spatial correlation ranges between 1.8 and 5 centimeters. The optical mean aperture, mean hydraulic aperture and mass balance aperture were all determined. In addition the coefficient of variation (C_v) and anisotropy ratio (AR) for each model was determined, to compare their predictions with the actual tracer behavior in each of the models. In all cases the hydraulically determined mean aperture was the same order of magnitude as the optically determined mean aperture. The mass balance derived mean aperture differed significantly from the optical mean aperture based on the degree of channeling in the model. However, neither the C_v nor the AR correlated well to the actual behavior of the tracers, suggesting they are insufficient to predict void connectivity. Overall the epoxy replicas preformed moderately well and can be well characterized for use in studies where visualization is of primary importance.

Keywords: fractured rocks; groundwater flow; physical modeling; aperture statistics

1. Introduction

An important distinction between flow in porous media and flow in fractured media is that in fractured media, only the plane of the fracture is available for the development of significant flow paths. The hydraulic conductivity of the rock matrix is often so low, on the order of 4.0 x 10^{-6} – 8.0 x 10^{-9} meters per second for the dolomites used in this study, that it effectively confines the mobile fluids to the void space of the fracture. Therefore accurate conceptualization of the distribution of flow paths within a fracture is of great importance when modeling this type of flow.

Assuming that variations in aperture size in natural fractures are negligibly small in comparison to the overall fracture length, early workers (e.g. Snow, 1965; 1968; 1969) modeling flow behavior in single fractures assumed that fracture walls could be represented by a parallel-plate model. Following this line of logic, laminar flow of an incompressible fluid between two parallel flat plates can be described by the steady-state solution to the Navier-Stokes equations for laminar flow (Romm, 1966; Witherspoon et al., 1980):

$$Q = \frac{-\rho g}{12 \mu} b_h^3 \frac{W}{L} \Delta h; \qquad [1]$$

where Q is the volumetric flow rate, ρ and μ are the density and viscosity of the fluid respectively, g is the acceleration due to gravity, Δh is the change in hydraulic head through the flow domain, W is the fracture width, L is the fracture length, and b_h is the distance between the parallel plates (i.e. the aperture). This equation is frequently referred to as the "cubic law" (Witherspoon et al., 1980), and it suggests that the only impediment to characterizing flow in rough-walled fractures is the accurate characterization of the effective hydraulic aperture (b_h).

Mean aperture or *hydraulic aperture* are the terms typically applied to describe the aperture determined from the results of flow experiments by calculation using the cubic law. In this work the term *hydraulic aperture* will always refer to the aperture (b_h) determined using the cubic law.

Another method to calculate the hydraulic equivalent aperture is based on tracer tests through the fracture, described by Tsang (1992). A *mass balance aperture* is determined using the relation $Qt_w = Ab_m$, where Q is the volumetric flow rate, t_w is the mean residence time of the tracer transport as determined from the first time moment of the measured breakthrough curve, A is the aerial extent of the fracture and b_m, is the mass balance aperture thus determined. Tsang argues that the mass balance aperture should be greater than or equal to the cubic law aperture. This relative size relationship occurs because of the variability of fracture apertures in real rough-walled systems. It is the smallest apertures within the fracture that control permeability as measured using the cubic law, while mass balance tracer tests reflect the influence of the large aperture channels, through which the solute migrates (Tsang, 1992). Tsang found the mass balance aperture to be a good estimate of the arithmetic mean of all the apertures in the fracture.

However, since fractures clearly are not smooth, parallel-plates, nor can they be assumed to behave as such over large areas (Brown and Scholz, 1985), the validly of the hydraulic equivalent aperture approach has been challenged by a variety of authors (e.g. Tsang and Tsang, 1987; Pyrak-Nolte et al., 1988; Moreno et al., 1988; Tsang et al., 1988). Instead, evidence suggests that the variability of aperture within a natural fracture

Deleted: as

Deleted: are

has a significant effect on the hydraulic behavior of that fracture, as flow will tend to occur selectively through the largest apertures (Silliman, 1989).

Bourke (1987) demonstrated that the majority of flow in a fracture is limited to only a few channels which may occupy as little as 10% of the fracture plane. Similarly, Rasmuson and Neretnieks (1986) concluded that fluid flow was spatially isolated in only 10-20% of the fracture plane. Experiments at field scale suggest that there is a disparity in the fluid flux observed at different locations within the same fracture plane (Heath, 1985; Rasmuson and Neretnieks, 1986; Bourke, 1987). These results have given rise to the "channel flow" concept and are obviously at odds with the assumption that variations in aperture are negligible. Instead, it appears that an actual aperture distribution must be known in order to correctly interpret flow.

There have been a variety of studies to characterize the distribution of apertures in natural fractures, which can be grouped broadly into four categories: (1) calculation from measurements of surface roughness (Gentier, 1986; Barton and Hsieh,1989; Voss and Shotwell, 1990) (2) casting techniques (Gale, 1987; Pyrak-Nolte et al., 1987; Gentier et al., 1989; Billaux and Gentier, 1990) (3) creation of replicas (Hakami, 1988, 1995; Hakami and Barton 1990; Hakami and Larsson,1996) and (4) non-contact sensing techniques (Johns et al., 1993; Kumar et al., 1995). Most of these groups, with certain reservations, established that their apertures were normally or more often lognormally distributed.

Neither surface roughness measurements, nor casts can be used for physical flow experiments. Thus, there are only two approaches to visualizing flow in a fracture of known aperture distribution. The first is through the creation of replicas, such as epoxy casts, the second is though the use of non-contact sensing techniques such as magnetic resonance imaging (MRI). The latter approach is prohibitively expensive for many research groups whose primary goal is to conduct visualization experiments. An additional advantage to the replica approach is that the surface chemistry of epoxy models can be systematically altered, allowing for multiple examinations of the same aperture distribution at differing degrees of wettability (Bergslien et al., 2004). Thus, the goal of the present study is to present a detailed description of an epoxy model creation process and present a brief geostatistical analysis of the models created. The models in this study were created for use in non-aqueous phase liquid flow studies (Bergslien and Fountain, 2006).

2. Methodology:

Samples of unweathered, fractured rock were collected from exposed sections of the Gasport, Goat Island, and Eramosa Formations of the Lockport Group from a variety of quarries located in western New York and Ontario, Canada. The Lockport Group is a Silurian age upwardly shallowing depositional carbonate sequence consisting, in the Niagara region of New York State and Ontario, Canada, of 49 – 54 meters (160 – 175 feet), of massive to medium-bedded dolomite with minor amounts of dolomitic limestone and shale (Brett et al., 1995). The Lockport Dolomite is pervasively fractured and is contaminated by non-aqueous phase liquids (NAPLs) at numerous sites throughout the Niagara Falls and neighboring regions.

Samples of various sizes with visible, unopened fractures were collected at field sites in western New York and southern Ontario, Canada. These samples were cut into

Comment [EB1]: These are stratigraphic units and I have referred to them using normal terminology. I am not sure what you want me to do to – what is the standard for your journal when referencing geologic units ? The Lockport Group is a geologic unit that reaches from the middle of New York State under the Great Lakes into Canada and out into Ohio, each of the names refers to a specific section of the Lockport group, not to a geographic location.

Deleted: o

rectangles using a diamond blade rock saw before being opened along the fracture plane by the slow application of shear stress using an off-set vise and a set of small wedges (Figure 1a). Samples which displayed significant weathering were discarded. Fracture types collected consisted of bedding plane fractures, stylolitically controlled fractures, vertical fractures, and fractures with secondary mineral infill.

Deleted: use

Using a method based on the work described in Persoff and Pruess (1995), and Hakami and Barton (1990), which was in turn based on Gentier (1986), a fracture casting technique was developed for the creation of translucent plastic models of natural fractures. The prepared rock samples were heated for approximately one hour at 50°C in a constant temperature cabinet. The samples were then removed from the oven and the exposed fracture surfaces were coated with a thin layer of vacuum degassed two-part silicone rubber, which was allowed to cure for several hours. Heating the rock significantly improves the flow of the silicone into the rough fracture surface. The silicone used in this study is specially designed for mold making and small parts casting, and can create molds with “precision surface detail up to 1 micron” (Silpack Inc., 1996).

To create the mold, a rigid steel tray was filled with vacuum degassed silicone to a depth sufficient to ensure that the entire rock fracture surface would be at least 1 cm below the surface of the silicone. The coated fracture was immersed in the silicone slowly at an angle to allow air to escape (Figure 1b). The mold was allowed to cure for a minimum of 24 hours at room temperature. Then to increase the rigidity of the mold and to ensure that it was free of excess moisture, the mold was given an hour long post cure treatment at 150°C with the rock still in place (Figure 1c). After the post cure, the rock

Deleted: will

Deleted: is

Deleted: is

Deleted: is

Deleted: is

was removed from the silicone mold, the surface gently cleaned and the mold was stored in a desiccant chamber (Figure 1d).

The fracture cast was created using Stycast 1267 two-part epoxy resin (Robert McKeown Co.). This epoxy is related to the Eccobond 27 epoxy used in several past studies in the literature, which was manufactured by W.R. Grace Company prior to 2001. The epoxy was mixed and vacuum degassed before being poured into a cleaned silicone mold in several thin layers, each of which was allowed to cure before the addition of the next layer (Figure 1e). After the final layer of epoxy was poured the cast was allowed to cure for a minimum of 24 hours in a desiccant chamber, and then post cured at 150°C for one to one and a half hours (Figure 1f). The post cure is essential for increasing the rigidity of the model. The casts were then removed from the mold and stored in a desiccant chamber until use (Figure 1g).

The transparent fracture casts were assembled to form a model of the natural fracture (Figure 1h). A heat molding process was used to ensure that the model had a tight fit. The assembled model was placed in a press with an average of 5 g/cm^2 applied to the models. This was the maximum pressure that could consistently be applied to the models without causing the casts to adhere to each other. Use of this process significantly improved the rigidity of the models, without significantly effecting the aperture distribution. The assembled model was then heated to 75°C for three hours and then allowed to cool for a minimum of 24 hours before it was removed from the press.

Several attempts were made to find a method to macroscopically quantify the accuracy of these models, including manual and laser profilometry, and digital topographic analysis but, to date, no satisfactory method of analysis has been found. In

Deleted: is
Deleted: mold
Deleted: is
Deleted: it
Deleted: is
Deleted: is
Deleted: is
Deleted: is
Deleted: is
Deleted: is
Deleted: are
Deleted: are
Deleted: is
Deleted: has
Deleted: is
Deleted: is
Deleted: is

the words of Brown et al. (1998) "the final epoxy replicas were checked for quality of reproduction … by hand fitting them to each other and comparing these to the fit of the two original rock surfaces."

In the final stage of preparation, the epoxy replica was reassembled to form a model of a natural fracture. The model was sealed along two opposite edges using Evercoat Formula 27 All-Purpose Filler, a two-part polyester resin which is water-proof and has no shrinkage, to form no-flow boundaries. The remaining sides were turned into source and sink areas using channeled plastic, which allowed uniform flow of water into and out of the fracture edges. Assembled models were flooded with CO_2 for a minimum of one hour before liquid saturation.

Deleted: preparation
Deleted: is
Formatted: Indent: First line: 36 pt
Deleted: is
Deleted: are
Deleted: allows
Deleted: are
Deleted: ¶
Deleted: ¶

3. Aperture Distribution Measurements

Aperture distribution within the fracture models was determined using a light transmittance technique by applying the Beer-Lambert law to the adsorption of light through fractures filled with dyed liquid. The Beer-Lambert law states that the absorbance of light (A) thought a dyed medium is equal to the product of the molar absorptivity of the dye (a), the path length or in this case the fracture aperture parallel to the incident light, (b), and the concentration of the dye (c) (Denny and Sinclair, 1987). Molar absorptivity is a constant for a particular compound in a particular solvent at a set wavelength, and dye concentration is a controlled constant. This leaves absorbance and path length the only variables.

Deleted: is

Because the Beer-Lambert law is technically only valid for polar, monochromatic light, a specially designed light box, which uses a mirror apparatus to direct parallel incident light to the camera, and a band-pass filter array, which lets only a very narrow range of wavelengths pass into the camera, was used to come as close to these restrictions as possible (Figures 2). This entire apparatus was also encased in blackout cloth to block all stray light. For the law to be valid the relationship between absorbance and path length must be linear, and with this equipment, it is possible to establish a linear relationship between absorbance and path length (in this case aperture), using narrow band polychromatic light (Figure 3).

Deleted: are

Deleted: is

Light attenuation was measured using a grayscale, 10-bit charge-coupled device (CCD) camera with 1030 x 1300 resolution (DVC-1300 High Resolution Video Camera; DVC Company), by taking two still images of the fracture model, one with the fracture filled with water and one with the fracture flooded with a dye of known concentration. The dye standard, denoted 100% Liquitint standard, was created using 1mL Liquitint Blue HP dye from Milliken Chemical per 1L of distilled water. CCD response is inherently linear, eliminating camera response as a potential erratic variable (Russ, 1995). The dyed image was divided by the water image to get transmittance (T), which is converted to absorbance by applying the relationship $A = \log_{10}(1/T)$ (Denny and Sinclair, 1987). Absorbance was converted to aperture at each pixel of the fracture, by correlating the absorbance values for the fracture image to the absorbance values for test cells of known separation distance using a calibration curve (Figure 2). Using this method it is possible to achieve a working accuracy of approximately +/- 0.005 millimeters.

Deleted: is

Deleted: is

Deleted: is

This method of calibrating aperture directly to transmittance is significantly different from the one developed by Detwiler et al. (1999), in which the measured aperture field was not related to a calibration curve, but was instead quantified using a series of images of known dye concentration and the authors presented a method of minimizing measurement error statistically.

Deleted: is

Deleted: is

A set of five replicas of natural fractures were used in this study (Table 1). For each of the fracture models, the mean aperture for each pixel in their computer-generated images was calculated using Scion Image, a Windows based version of NIH Image (National Institute of Health), and ENVI 3.4 (Research Systems, Inc.). The optical aperture distribution matrix for each of the models was created using the basic math function of ENVI 3.4 and the appropriate calibration curve (Figure 3). In all cases one pixel is approximately equal to 140 microns in both the x (left to right) and y (top to bottom) directions (Figure 4).

Deleted: computer generated

Deleted: is

From each data set an arithmetic mean optical and geometric mean optical aperture was determined for each replica (Table 2). The geometric mean aperture (b_{geo}) is calculated from the following relationship:

$$b_{geo} = \left(\prod_{i=1}^{n} a_i \right)^{1/n} \qquad [2]$$

where n is the number of data points in the matrix and a is the value of each individual data point.

The coefficient of variation (C_v) for each fracture was also determined (Table 2). The C_v, which is an indicator of fracture heterogeneity, is defined as the ratio of the standard deviation to the arithmetic mean aperture (Lee et al., 2003). Higher C_v values are indicative of greater deviation from the parallel plate model, thus more tortuous flow and greater solute dispersivity.

For comparison the mean hydraulic aperture and the mass balance aperture were also determined for each of the replicas (Table 2). The hydraulic aperture (b_h) is determined using the cubic law as follows:

$$b_h = \sqrt[3]{\frac{12\mu \mathrm{Q}}{\rho\, \mathrm{g}\, \Delta \mathrm{h}}\left(\frac{L}{W}\right)}; \qquad [3]$$

variables as defined previously [1] (Tsang, 1992). The cubic law can be used as a first order approximation of the average fracture aperture, but in rough walled fractures actually represents a complex geometric mean that is weighted towards the smaller apertures (Tsang, 1992; Oron and Berkowitz, 1998). Brown (1984) suggested that the hydraulic aperture for an isotropic aperture field should actually be equal to the geometric mean of the aperture distribution, thus theoretically the greater the deviation between b_{geo} and b_h, the greater the likelihood of anisotropy.

The mass balance aperture (b_m) was calculated using tracer tests using a 1000ppm (parts per million) sodium bromide solution. Head on each of the water-saturated replicas was adjusted until a discharge rate of approximately 1mL per 18 seconds was achieved (except model RN9, which had a flow rate of approximately 1mL per 6 seconds. The inlet is then switched to the 1000ppm NaBr solution and a timer started. For each replica a one 5mL sample of the effluent was taken every 90 seconds and mixed with

Deleted: are

Deleted: is

Deleted: is

Deleted: is

Deleted:

Deleted: O

5mL of room temperature distilled water using a stir bar. The bromide concentration of each effluent sample was determined using an Orion 290A portable pH/ISE (ion specific electrode) meter with a bromide ion selective electrode and a five-point calibration curve. Samples were taken until there had been several readings of approximately 500ppm, i.e. the full concentration of the injected tracer (Figure 5). The influent was then switched to distilled water, head increased and the replica flushed until there was no detection of bromide in the effluent.

Comment [MSOffice2]: defines ISE

Deleted: is

Deleted: are

Deleted: ve

Deleted: is

Deleted: is

Mass balance aperture (b_m) is determined using the following relationship:

$$b_m = Qt_w / LW \qquad [4]$$

where t_w is the mean residence time of tracer transport as determined from the time moment of the measured breakthrough curve and the other variables are as defined previously (Tsang, 1992). The mean residence time of the tracer (t_m) is found from the relationship:

$$t_m = \frac{\int_0^\infty t\, C(t)}{\int_0^\infty C(t)}; \qquad [5]$$

as described in Gaspar (1987). The time delay (t_{dv}) as the tracer moves though dead volume (V_{dv}), such as empty tubing, was calculated for time correction. It is assumed that no dispersion occurs in the dead volume (V_{dv}), therefore $t_{dv} = V_{dv}/Q$, leading to the corrected mean residence time $t_w = t_m - t_{dv}$.

The mass balance aperture (b_m) represents the true arithmetic mean of the aperture distribution, and therefore should always be larger than the hydraulic aperture. In essence, while small apertures control the permeability and thus the hydraulic aperture of a fracture, the mass balance aperture is strongly influenced by the largest apertures which present the most direct pathway for solute transport. Tsang (1992) found the mass balance aperture to be a very good estimate of the "equivalent aperture" for single fractures.

Deleted: will

4. Statistical Parameters

Statistical analysis of the optically determined aperture matrices showed a skew towards smaller apertures. In general, the larger models (RN3, RN4, RN9) appear to have lognormal aperture distributions (R^2 values 0.95, 0.92 and 0.88 respectively), and the smaller models (S1, SRN31) appear to have normal aperture distributions (R^2 values of 0.97 and 0.93 respectively).

Surface variograms of each of the models were created based on a spherical model, by randomly selecting 200 points out of each of the data sets and using GS+ (Gamma Design Software). Surface variograms are used to give a general overview of the anisotropy of the data and to aid in the identification of the major and minor axes of anisotropy (Isaaks and Srivastava, 1989). Each of the surface variograms produced in this study displays a significant degree of anisotropy and suggests that replica RN3 displays the highest degree of roughness, while RN4 displays the least roughness. These results appear to be somewhat at variance with those of Hakami (1995), that the greater the surface roughness of the fracture the more likely it will fit a lognormal distribution. In that case, replica S1 or SRN1 should have showed the least surface roughness.

Deleted: s

Omnidirectional and directional semivariograms for each of the replicas were created with Gstat (Pebesma &Wesseling, 1998) using the best-fit spherical model. There is a limited amount of data in the literature regarding the spatial correlation of apertures within a fracture plane. Gelhar (1993) suggests, based on stochastic analysis and field tracer tests, that fractures may have correlation lengths of less than a meter. Hakami (1995) found spatial correlation lengths from 1 to 5 centimeters. On the other hand, Vickers et al. (1992) believe that fractures are actually autocorrelated at two scales; on the order of a few millimeters and on the order of tens of centimeters. Kumar et al. (1995) used nuclear magnetic resonance imaging techniques to measure aperture and suggest that apertures are correlated over lengths on the order of one centimeter. The omnidirectional semivariograms for this study indicate that the fracture replicas have spatial correlation ranges between approximately 1.8 and 5 centimeters (Table 3), which compares well with the results reported by Hakami (1995) and Kumar et al. (1995).

Deleted: best fit

The directional variograms generated confirm that the models all have some degree of anisotropy, with SRN31 having the greatest degree and both RN4 and RN9 having the lowest degree. The anisotropy ratio (AR), defined as the ratio of the longitudinal correlation length (λ_L) to the transverse correlation length (λ_T), is another method of characterizing the overall degree of anisotropy of the aperture distribution (Lee et al., 2003) (Table 3).

5. Results and Conclusions

In all cases the hydraulically determined mean apertures of the replicas used in this study were the same order of magnitude, but an average of 300µm smaller than the optically determined arithmetic mean aperture. This is unsurprising, as the smallest apertures control the hydraulic mean aperture, and agrees with the supposition of Tsang (1992).

The optical geometric mean apertures were on average 190µm larger than the hydraulically determined mean apertures. The greatest difference was for model SRN31 while the least difference was for model RN3. Based on the statistical analysis, replica SRN31 actually displays the highest degree of anisotropy, while RN4 and RN9 display the least. This is almost the reverse of the prediction based on difference from geometric mean, indicating that it cannot be used predicatively in this way.

Deleted: backward

The mass balance derived average apertures had the most variation. According to Tsang (1992), the mass balance aperture should represent the pore volume of the fracture and be a true arithmetic mean of the actual aperture distribution, represented here by the optical arithmetic mean aperture. For models RN3 and RN9, the largest models spatially, there is good agreement between the optically determined arithmetic mean apertures and the mass balance mean apertures (Table 3). This suggests the least channeling and lower surface roughness for these models. However, replica RN3 has the highest C_v (0.94) out of all of the models, and the surface variogram indicates this model should have the greatest surface roughness out of all of the models. The AR for RN3 is moderate (0.59) again suggestive of some degree of channeling. Replica RN9, on the other hand, has a moderate C_v (0.63) and the AR is close to unity, which is more in keeping with the results of the tracer test.

For model RN4, the mass balance aperture is roughly double the optical arithmetic mean aperture, though still of the same magnitude (Figure 6). It has been demonstrated in several studies that mean fracture apertures derived from tracer tests can be as much as 2 to 3 orders of magnitude higher than hydraulic mean apertures (e.g. Neretnieks, 1993; Shapiro and Nicholas, 1989). The general assumption is that while hydraulic mean apertures are strongly controlled by the smallest apertures, solvents will preferentially travel though the largest apertures, potentially resulting in significant discrepancies between the two measures of aperture. The C_v of RN4 is quite high (0.81), suggesting a high degree of surface roughness and significant channeling, which agrees with the results of the tracer tests. The AR, which is identical to that of replica RN4, is close to unity, indicating a low degree of anisotropy.

Model S1, the smallest of the replicas used, had a mass balance mean aperture slightly less than three times greater than the optically determined arithmetic mean aperture (Figure 7). The tracer test on this model was repeated, with the same results. Based on the results of the tracer tests, while replica S1 has the smallest hydraulic mean aperture, there is a zone of connected high aperture void space that allows for rapid solute transport. This finding would suggest that S1 should also have a high degree of surface roughness and anisotropy, though the measures applied, C_v and AR, appear contrary to this. Replica S1 has the lowest C_v (0.48) implying that the fracture displays the least heterogeneity and therefore the least channeling. The anisotropy ratio calculated for S1 is

0.51, close to the value for RN3 (0.59), which has behaved completely the opposite with very similar optical arithmetic and hydraulic mean apertures.

Model SRN31 is the second smallest of the models and has a normal aperture distribution, similar in character to S1 (Figure 8). Also similar to S1, the mass balance was approximately two times larger than the optical arithmetic mean aperture. Again this would suggest that there is a significant channeling effect that allows rapid solute transport. Replica SRN31 did have the anisotropy ratio that deviated most from unity (0.33), which indicates a high degree of anisotropy, though the C_v (0.68) suggests only a moderate degree of surface roughness.

Thus, neither of the geostatistial approaches examined, C_v and AR, appear to be good predictors of tracer behavior in the replicas examined. There was no correlation between the results of these measures and the actual behavior of the tracer in the models. This suggests that these measures, while reflective of some of the physical properties of the fractures, are insufficient to capture the connectivity of the void space.

Overall the models compare well with other results found in the literature (Table 4). The major deficiency of these models is due to the inherent flexibility of the epoxy, which has a tendency to bow when large sections are unsupported. For small models, less than 20 cm x 20 cm, the casting method presented ensures sufficient rigidity that deformation is minimized. The smaller models (S1 and SRN31) experienced less than a 1% change in aperture distribution over time, while the larger models experienced less than an 8% change, on average; the larger the area of the model, the greater the potential for deformation.

The application of a compressive force to the models during experiments would help alleviate this problem and increase the scope of these studies. A larger model with small metal frame was created in an attempt to compress the central regions of the models, but it was only useful for a short period of time and partially defeated the purpose of creating transparent models. Compression between two sheets of glass or within a hydraulic mechanism might be a more useful approach. Without such support, this limits the utility of this approach to models that are at maximum approximately 30 cm x 30 cm. Another obstacle to scaling up epoxy models is the exothermic reaction of curing epoxy, large volumes of which will experience uneven curing, which destroys surface roughness detail, and causes bubbling in the plastic.

There are currently few approaches available to researchers interested in visualization of flow and transport in fractures. While the epoxy model approach has some significant deficiencies, it is currently the cheapest and most flexible of the available physical modeling approaches. The degree of accuracy with which the models replicate actual fracture surfaces is an active matter of debate, and to date there is no commonly available technology to characterize actual fracture apertures for comparison. One strength in the epoxy model approach lies in the ease of fully characterizing the models, so that any visualization experiments can be conducted in a well-characterized aperture field. Researchers must weigh the deficiencies of the method against the benefits of utilizing a low cost visualization method (verses magnetic resonance imaging etc.) for the task at hand.

Deleted: M

Deleted: R

Deleted: I

Formatted: Font: Bold

Acknowledgements: The initial stages of this work were performed at the University at Buffalo with pilot grants from the Mark Diamond Fund and the Geological Society of America. A Research Incentive Grant from the Research Foundation at Buffalo State College assisted in the completion of this study. The authors would like to thank the above organizations and to thank the reviewers and editors who have helped bring this article to press.

References

Barton C. C., and P.A. Hsieh. (1989) Physical and Hydrological Flow Properties of Fractures *in Field Trip Guidebook T385*, 36 p.

Bergslien, E.T., Fountain, J.C. and Giese, Jr. R. (2004) Characterization of the surface properties of epoxy-type models used for multiphase flow studies in fractured media and creation of a new model, *Water Resources Research*. Vol. 40 (5), W05112.

Bergslien, E.T., and J.C. Fountain (2006) The effect of changes in wettability on two-phase saturated flow in horizontal replicas of single natural fractures, *Journal of Contaminant Hydrology*, 88(3-4), 153-180.

Billaux, D., and S. Gentier. (1990) Numerical and Laboratory Studies of Flow in a Fracture, *in Proceedings of the International Conference on Rock Joints*, Loen, Norway. Rotterdam: Balkema, pp. 369-374.

Bourke P. J. (1987) Channeling of flow through fractures in rock *in Proceedings of GEOVAL-87 International Symposium*.

Brett, C.E., D.H. Tepper, W.M. Goodman, S. T. LoDuca, and B. Eckert (1995) *Revised Stratigraphy and Correlations of the Niagaran Provincial Series (Medina, Clinton, and Lockport Groups) in the Type Area of Western New York.* U.S. Geological Survey Bulletin 2086, 66 pp.

Brown, D.M. (1984) Stochastic analysis of flow and solute transport in a variable-aperture rock fracture. M.S. thesis, Mass. Inst. Of Technology, Cambridge.

Brown, S., A. Caprihan, and R. Hardy. (1998) Experimental observation of fluid flow channels in a single fracture. *Journal of Geophysical Research*. 103(B3): 5125-5132.

Brown S. R., and C.H. Scholz. (1985) Closure of random elastic surfaces in contact. *Journal of Geophysical. Research*. 90(B7), 5531-5545.

Denny R. C. and R. Sinclair (1987) *Visible and Ultraviolet Spectroscopy*. John Wiley and Sons.

Detwiler, R. L., S.E. Pringle, and R.J. Glass (1999) Measurement of fracture aperture fields using transmitted light: An evaluation of measurement errors and their influence on simulations of flow and transport through a single fracture. *Water Resources Research,* 35(9), 2605 – 2617.

Gale J. E. (1987) Comparison of coupled fracture deformation and fluid flow models with direct measurements of fracture pore structure and stress-flow properties *in Proceesings of the 28th U.S. Symposium on Rock Mechanics*, 1213-1222.

Gale J. E. (1990) Hydraulic behavior of rock joints *in Rock Joints, Proceedings of the International Symposium on Rock Joints*, 351-362.

Gaspar, Emilian (1987) *Modern Trends in Tracer Hydrology.* CRC Press Inc., 145 p.

Gelhar L. W. (1993) *Stocastic Subsurface Hydrology*. Prentice Hall, 390 pp.

Gentier S. (1986) *Morphologie et comportement hydromecanique d'une fracture naturelle dans un granite sous contrainte normale (Hydromechanical morphology and behavior of a natural fracture in a granite under normal stress)*. Ph.D., Univ. d'Orleans, France

Gentier S., Billaux, and L. Van Vliet. (1989) Laboratory testing of the voids of a fracture. *Rock Mechanics* 22, 149-157.

Formatted: Font: Italic

Hakami, E. (1988) Water flow in single rock joints. Licentiate Thesis, Luleå University of Technology, Luleå, Sweden.
Hakami, E. (1995) *Aperture Distribution of Rock Fractures.* Ph.D., Royal Institute of Technology, Stockholm, Sweden.
Hakami E., and N. Barton. (1990) Aperture measurements and flow experiments using transparent replicas of rock joints in *Proceedings of the First International Symposium on Rock Joints*, 383-390.
Hakami, E., and E. Larsson (1996) Aperture measurements and flow experiments on a single natural fracture. *International Journal of Rock Mechanics, Mining Sciences and Geomechanics abstracts.* 33(4), 395 – 404.
Heath, M.J. (1985) Solute migration experiments in fractured granite, South West England, in design and instrumentation of in situ experiments in underground laboratories for radioactive waste disposal, *in* A.A. Balkema (ed.) *Proc. of a Joint CEC-NEA Workshop,* pp. 191 – 200.
Isaaks, E.H. and R.M. Srivastava (1989) *An Introduction to Applied Geostatistics.* Oxford University Press, New York, New York. 561p.
Johns R. A., J.S. Steude, L.M. Castanier, and P.V. Roberts. (1993) Nondestructive measurements of fracture aperture in crystalline rock cores using X-ray computed tomography. *J. Geophys. Res.* 98(B2), 1889-1900.
Kumar A. T. A., P.D. Majors, and W.R. Rossen. (1995) Measurement of aperture and multiphase flow in fractures using NMR imaging *in Proceedings of SPE Annual Technical Conference and Exhibition*, SPE Paper 30558.
Lee, J., M. Kang, and J. Choe (2003) Experimental analysis on the effects of variable apertures on tracer transport. *Water Resour. Res.* 39(1), 1015, doi:10.1029/2001WR001246.
Moreno L., Y.W. Tsang, C.F. Tsang, F.V. Hale, and I. Neretnieks. (1988) Flow and tracer transport in a single fracture: a stocastic model and its relation to some field observations*. Water Resour. Res*. 24(12), 2033-2048.
Neretnieks, I. (1993) Solute transport in fractured rock – Applications to radionuclide waste repositories, *in Flow and Contaminant Transport in Fractured Rock*, eds. J. Bear, C.F. Tsang, and G de Marsily, Academic Press, San Diego, CA, pp. 39-127.
Oron, A.P. and B. Berkowitz (1998) Flow in rock fractures: the local cubic law assumption reexamined. *Water Resources Research.* 34(11), 2811 – 2825.
Pebesma, E.J. and C.G. Wesseling (1998) Gstat, a program for geostatistical modelling, prediction and simulation. *Computers & Geosciences* 24 (1), 17–31. Homepage http://www.gstat.org/index.html last accessed 08/14/2007.
Persoff P., and K. Pruess. (1995) Two-phase flow visualization and relative permeability measurement in natural rough walled fractures. *Water Resour. Res.* 31(5), 1175-1186.
Pyrak-Nolte L. J., L.R. Myer, N.G.W. Cook, and P.A. Witherspoon. (1987) Hydraulic and mechanical properties of natural fractures in low permeability rock *in Proceedings of the 6th International Congress on Rock Mechanics*, 225-231.
Pyrak-Nolte L. J., N.G.W. Cook, and D.D. Nolte. (1988) Fluid percolation through single fractures. *Geophys. Res. Letters* 15(11), 1247-1250.

Deleted: ¶

Rasmuson, A. and I. Neretnieks (1986) Radionuclide migration in strongly fissured zones; the sensitivity to some assumptions and parameters. *Water Resources Research.* 22(4), 559 – 569.

Raven K. G., and J.E. Gale. (1985) Water flow in a natural rock fracture as a function of stress and sample size. *Int. J. Rock Mech. Min. Sci. Geomech. Abstr*. 22, 251-261.

Romm E. S. (1966) *Fluid Flow in Fractured Rock*. (in Russian) 283 pp. Nedra, Moscow, Russia. Translated by the Phillips Petroleum Company in 1972, 283 p.

Russ, J.C. (1995) *The Image Processing Handbook 2nd Edition.* CRC Press, Boca Raton, Florida. 674p.

Shapiro, A.M. and J.R. Nicholas. (1989) Assessing the validity of the channel model of fracture aperture under field conditions. *Water Resources Research.* 25, 817 – 828.

Silliman S. E. (1989) An interpretation of the difference between aperture estimates derived from hydraulic and tracer tests in a single fracture. *Water Resour. Res*. 25(10), 2275-2283.

Silpack Inc. (1996) Silpack Inc. Technical Data Sheet, Pamona, CA., Silpack Inc. 4p.

Snow D. T. (1965) Parallel plate model of fractured permeable media. Ph.D., Univ. of Calif.

Snow D. T. (1968) Rock fracture spacings, openings, and porosities*. J. Soil Mech. Fdns. Div. Am. Soc. Civ. Engrs*. 94(SM1), 73-91.

Snow D.T. (1969) Anisotropic permeability of fractured media. *Water Resources Research.*5, 1273 – 1289.

Tsang Y.W. (1992) Usage of "equivalent apertures" for rock fractures as derived from hydraulic and tracer tests. *Water Resources Research.* 28(5), 1451-1455.

Tsang Y.W., and C.F. Tsang (1990) Hydrological characterization of variable-aperture fractures, *in International Symposium on Rock Joints*, A.A. Balkema, Brookfield, VT. pp. 423-430

Tsang Y. W., and C.F. Tsang. (1987) Channel model of flow through fractured media*. Water Resour. Res*. 23(3), 467-479.

Tsang Y. W., C.F. Tsang, I. Neretnieks, and L. Moreno. (1988) Flow and tracer transport in fractured media: a variable aperture channel model and its properties. *Water Resour. Res.* 24(12), 2049-2060.

Vickers B. C., S.P. Neumann, M.J. Sully, and D.D. Evans. (1992) Reconstruction and geostatistical analysis of multiscale fracture apertures in a large block of welded tuff. *Geophys. Res. Letters* 19(10), 1029-1032.

Voss, C.F. and L.R. Shotwell (1990) An investigation of the mechanical and hydrologic behavior of tuff fractures under saturated conditions. *in Proceedings of High Level Radioactive Waste Management.* American Nuclear Society. 825 – 834.

Witherspoon P. A., J.S.Y. Wang, K. Iwai, and J.E. Gale. (1980) Validity of the cubic law for fluid flow in a deformable rock fracture. *Water Resour. Res.* 16(6), 1016-1024

Figures:

Figure 1: Mold Creation and Casting Process. See text for description of the process. Figure not to scale.

Figure 2: Transmittance verses Wavelength for Experimental Setup

Figure 3: Linear Calibration Curves for LIQUITINT Blue Dye at three different concentrations

Figure 4: Optically Determined Aperture Distribution for Model RN3. Direction of flow indicated by arrow.

Figure 5: Bromide Breakthrough Curves shown in Normalized Concentration (Effluent Concentration divided by Initial Concentration)

Figure 6: Optically Determined Aperture Distribution for Model RN4. Direction of flow indicated by arrow.

Figure 7: Optically Determined Aperture Distribution for Replica S1. Direction of flow indicated by arrow.

Figure 8: Optically Determined Aperture Distribution for Model SRN31. Direction of flow indicated by arrow.

Comment [EB3]: This is just an illustration of the process, not a specific model, so I ca[illegible]y add a metric scale bar. I added [illegible]hat says "not to scale."

Comment [EB4]: I have spelled out standard and tried to clarify the curves.

Comment [EB5]: Absorbance is unitless. It is a ratio so the units cancel out and none should be listed

Tables:

Table 1 - Description of Fracture Models Used in Study

Model	RN3	RN4	RN9	S1	SRN31
Width (cm)	13.6	15.9	~20	7.9	6.5
Length (cm)	18.6	12.9	18.4	10.2	18.0
Volume (cm^3)	16	10	20	4.1	14
Fracture Type	Horizontal bedding plane	Horizontal bedding plane	Stylolitically controlled	Horizontal bedding plane	Stylolitically controlled

Table 2 – Statistical Parameters of Aperture Distribution of the Fracture Models

Model	RN3	RN4	RN9	S1	SRN31
Arithmetic Optical Mean Aperture (µm)	470	430	649	417	640
Standard Deviation	443	347	407	201	437
Coefficient of variation	0.94	0.81	0.63	0.48	0.68
Geometric Optical Mean Aperture (µm)	359	350	502	351	494
Hydraulic Mean Aperture (µm)	211	173	330	146	250
Mass Balance Mean Aperture (µm)	438	853	644	1168	1253

Table 3 – Geostatistical Analysis of Fracture Replicas

Model	RN3	RN4	RN9	S1	SRN31
Distribution	Lognormal	Lognormal	Lognormal	Normal	Normal
Correlation Length (cm)	1.8	3.2	4.0	2.0	3.5
Anisotropy Ratio	0.59	1.16	1.16	0.51	0.33
Magnitude of difference between optical geometric b and b_h (μm)	148	177	172	205	244
Magnitude of difference between optical arithmetic b and mass balance b_m (μm)	32	423	5	751	613

Table 4 – Some Measured Apertures of Single Fractures from the Literature

Author	Rock Type	Mean Aperture
Hakami and Barton (1990)	Leptite	313 µm / water drop areas
	Quartz monzonite	402 µm / water drop areas
		41 µm / water drop areas
		216 µm / water drop areas
	Fine grained granite	84 µm / water drop areas
		161 µm / water drop areas
Hakami and Larsson (1996)	Medium grained granite	360 µm / measurement of fluorescent epoxy fill 250 µm / hydraulic aperture
Kumar et al. (1995)	Limestone	265 µm / NMRI *
	Granite	192 µm / NMRI *
Lee et al. (2003)	Sandstone	250 – 384 µm / optically
Shapiro and Nicholas (1989)	Dolomite	2,150 – 2,700 µm / field test
Voss and Stockwell (1990)	Volcanic tuff	250 µm / optically

* NMRI - nuclear magnetic resonance imaging

Comment [MSOffice6]: please define NMRI here, or at the bottom of the table

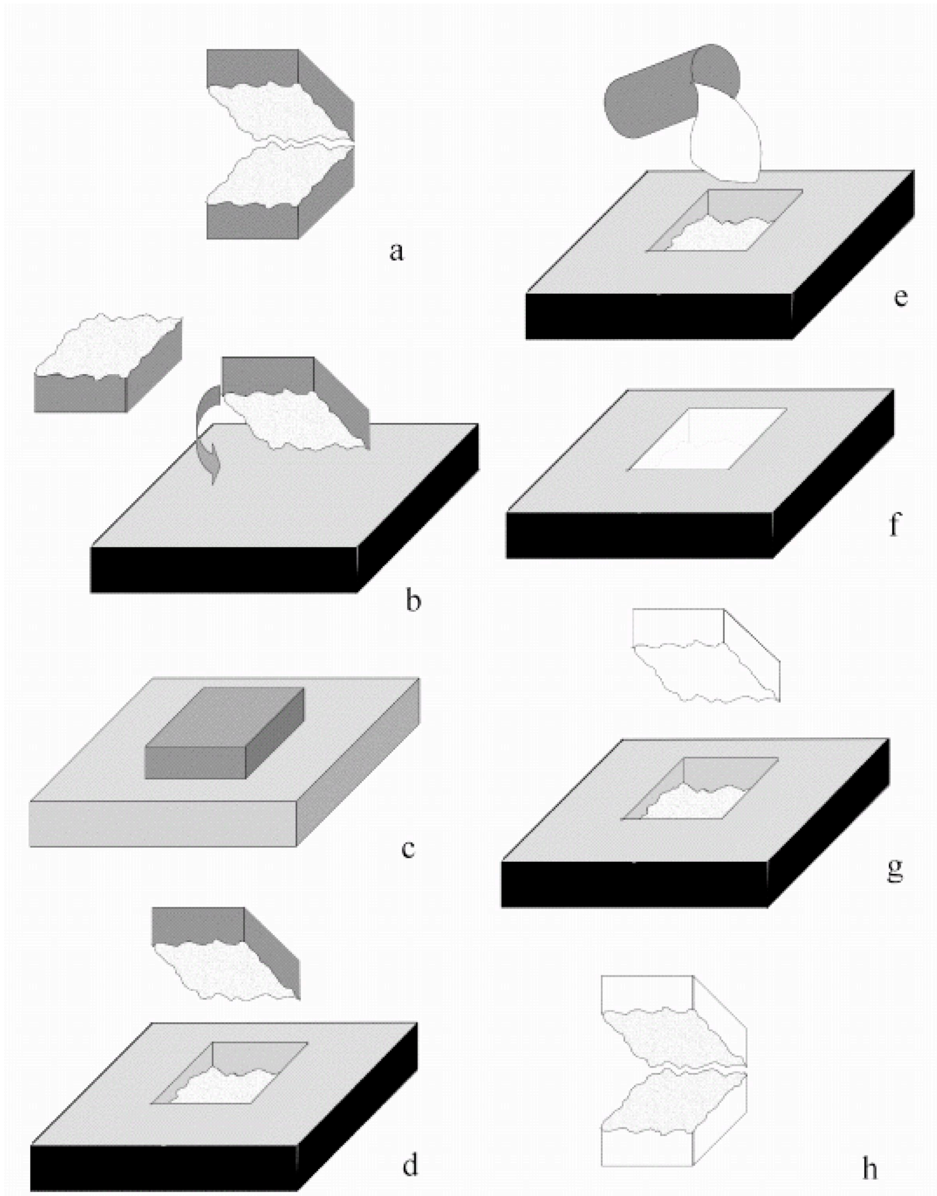

Figure 1: Mold Creation and Casting Process. See text for description of the process. Figure not to scale.
101x129mm (600 x 600 DPI)

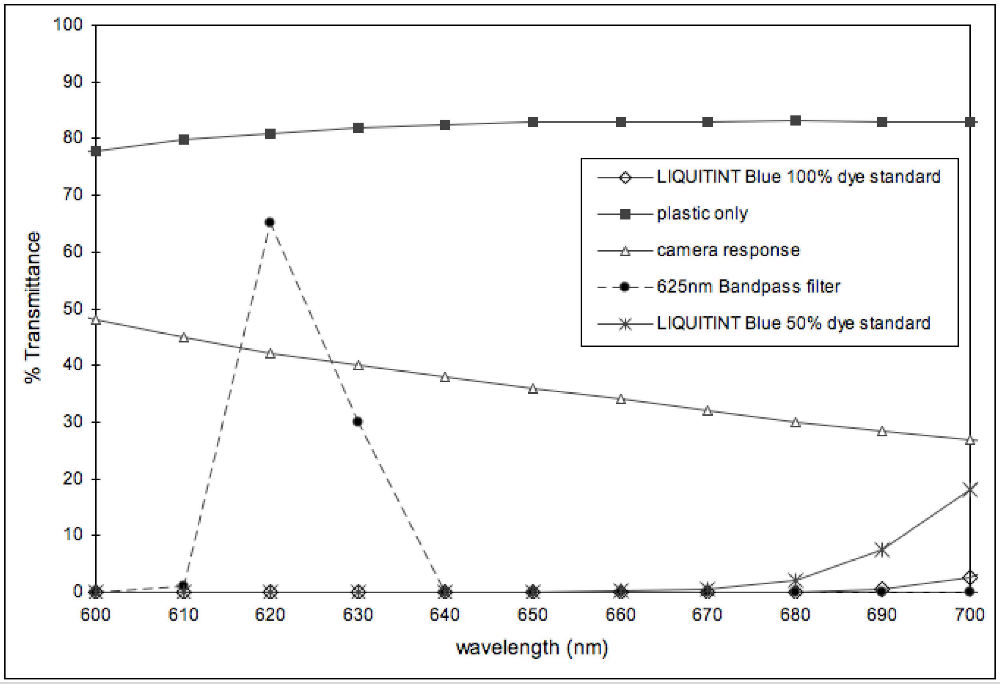

Figure 2: Transmittance verses Wavelength for Experimental Setup
130x90mm (600 x 600 DPI)

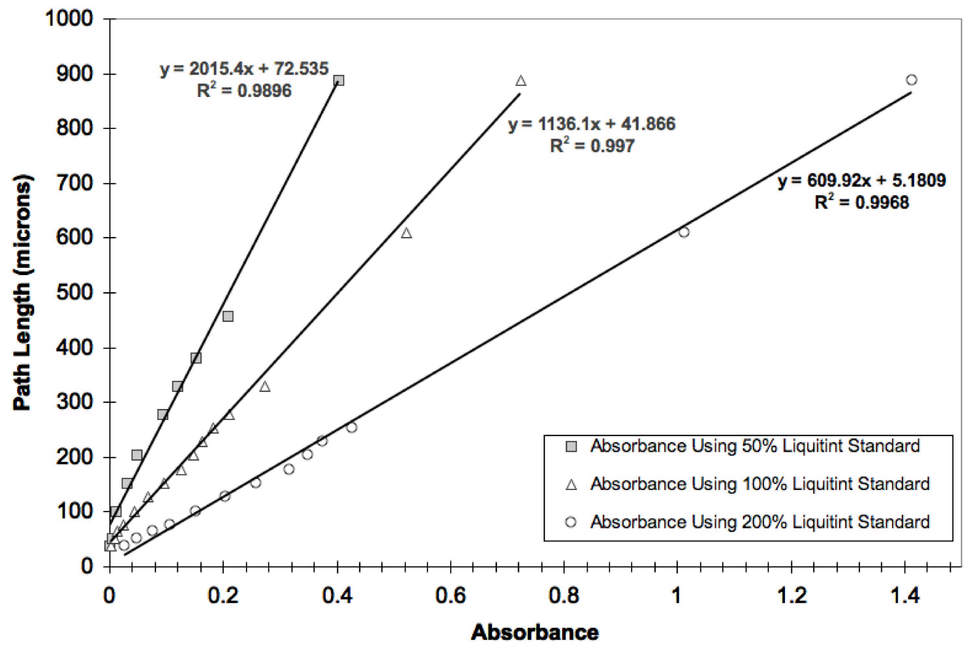

Figure 3: Linear Calibration Curves for LIQUITINT Blue Dye at three different concentrations
130x89mm (600 x 600 DPI)

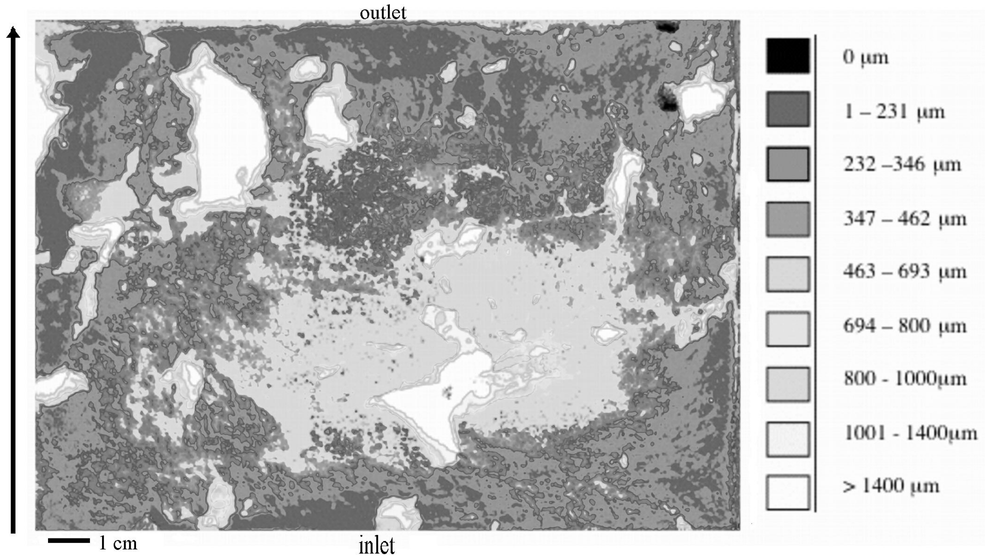

Figure 4: Optically Determined Aperture Distribution for Model RN3. Direction of flow indicated by arrow.
181x100mm (300 x 300 DPI)

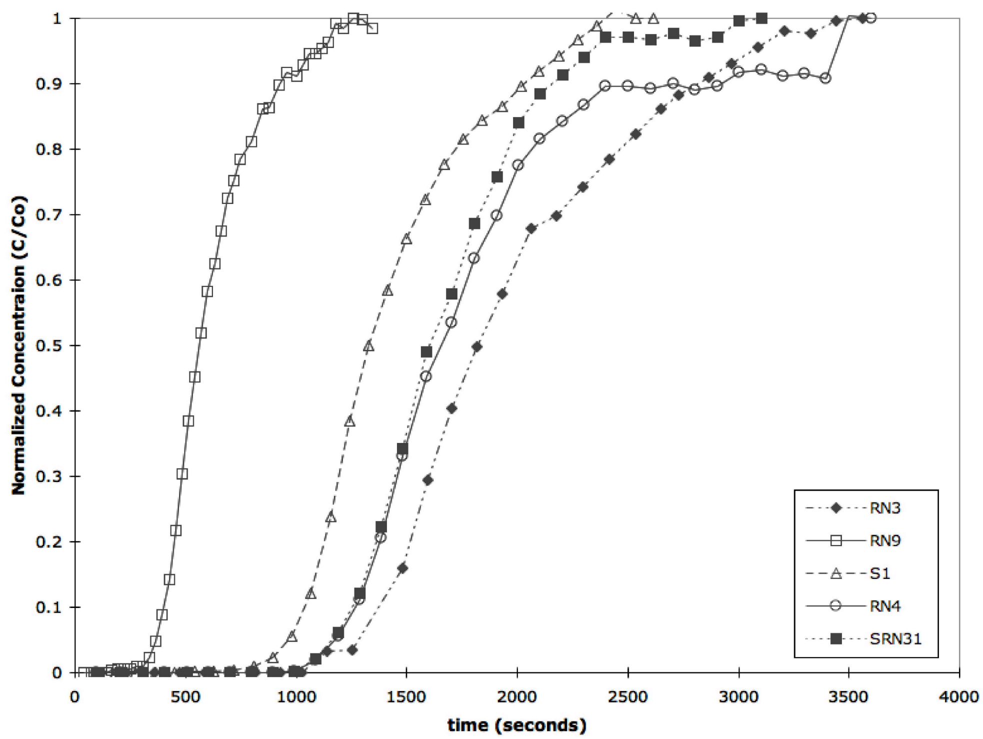

Figure 5: Bromide Breakthrough Curves shown in Normalized Concentration (Effluent Concentration divided by Initial Concentration)
130x98mm (600 x 600 DPI)

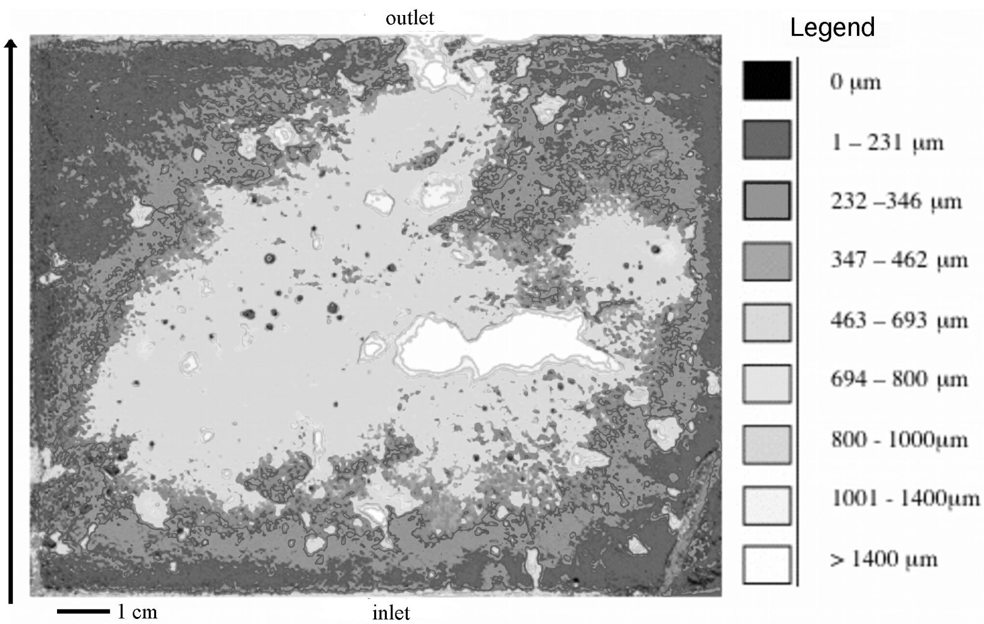

Figure 6: Optically Determined Aperture Distribution for Model RN4. Direction of flow indicated by arrow.
174x110mm (300 x 300 DPI)

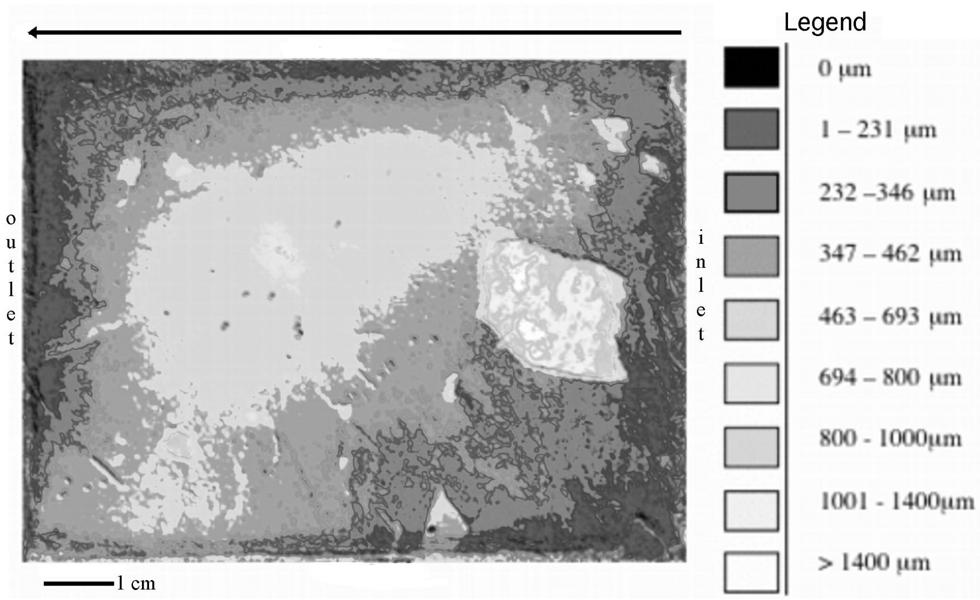

Figure 7: Optically Determined Aperture Distribution for Replica S1. Direction of flow indicated by arrow.
179x106mm (300 x 300 DPI)

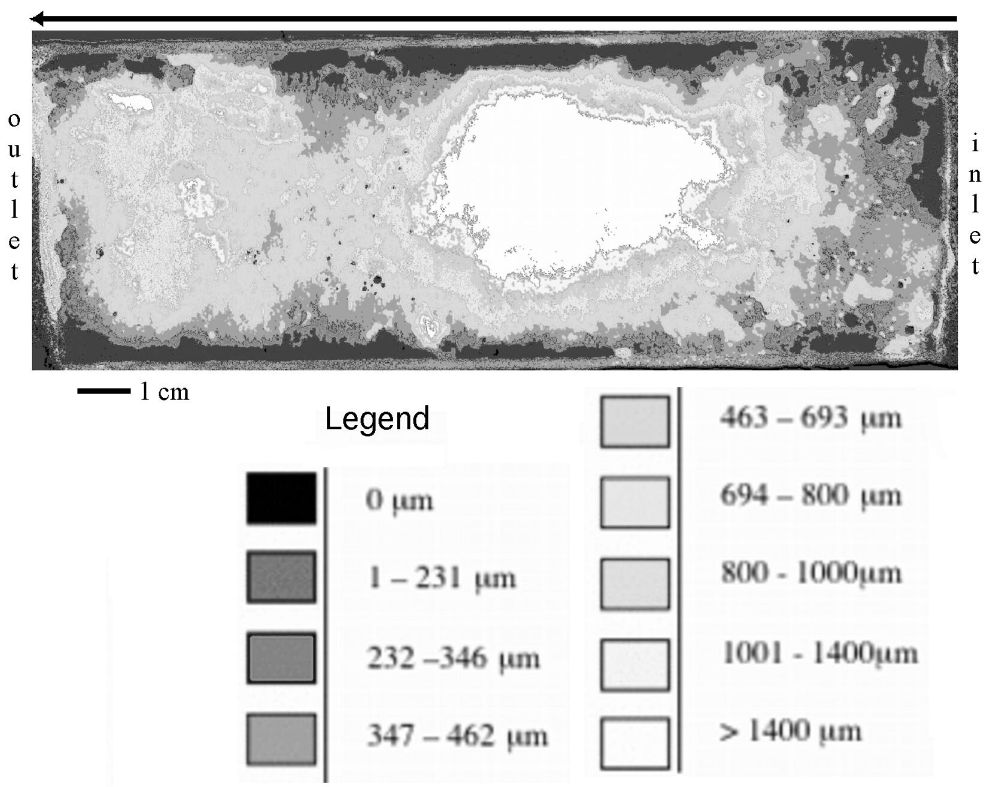

Figure 8: Optically Determined Aperture Distribution for Model SRN31. Direction of flow indicated by arrow.
141x111mm (300 x 300 DPI)